



# Improving tensile properties of glass fiber-reinforced epoxy resin composites based on enhanced multiphase structure: The modification of resin systems and glass fibers

Yinlong Cao<sup>a</sup>, Guanghui Gao<sup>a</sup>, Peng Zhang<sup>a</sup>, Jiuwen Bao<sup>a,\*</sup>, Peng Feng<sup>b</sup>, Rong Li<sup>c</sup>,  
Wenhuan Wang<sup>a</sup>

<sup>a</sup> School of Civil Engineering, Qindao University of Technology, Qindao 266000, China

<sup>b</sup> Department of Civil Engineering, Tsinghua University, Beijing 100084, China

<sup>c</sup> Central Research Institute of Building and Construction CO. LTD. MCC Group, China

## ARTICLE INFO

### Keywords:

Glass fiber-reinforced polymers  
Silane coupling agents  
Nanomaterials  
Resin systems  
Tensile properties

## ABSTRACT

Glass fiber-reinforced polymer (GFRP) composites have been widely used as reinforced materials in marine engineering due to their good corrosion resistance and economic benefits. However, the mechanical properties of GFRP are lower than that of composites reinforced by carbon and aramid fibers etc. Methods to improve the mechanical properties of GFRP received ongoing attention. GFRP have various mechanical properties due to the characteristics of its multiple phases. This study developed an optimized processing method based on multiphase structures for GFRP composites, significantly enhancing the tensile properties of GFRP laminates. The modified GFRP can be produced efficiently by this method to meet more utilization situations in marine engineering. The influence of curing agents, silane coupling agents (SCA)-treated glass fibers (GFs), and nanomaterials on GFRP's tensile properties was investigated. The findings reveal a 10.64 % increase in the characteristic load of GF bundles due to the improved bonding between fibers by SCA. Besides, the contact angle between SCA-treated GFs and epoxy resin shows a significant reduction (26.69 %). Variations in ply thickness and resin system distinctly influence the tensile properties and failure modes of GFRP laminates. Laminates with 4-ply GF fabrics facilitate more effective load transfer across the matrix-fiber boundary, yielding optimal tensile properties for GFRP. Epoxy/phenolic amine resin system with more reactive functional groups (-OH) enhances the fiber-resin bonding, further improving the tensile properties of GFRP. The enhancement mechanism of the multiphase structure in GFRP was elucidated by microscale characterization, indicating that the multiphase structures in GFRP, enhanced by SCA, nanomaterials, and functional curing agents, significantly improve its tensile properties.

## 1. Introduction

Fiber-reinforced polymer (FRP) composites have multiple phases, including fibers, resin, and an interfacial phase. Each phase's unique characteristics contribute to the mechanical properties of FRP composites [1,2]. Methods to improve the mechanical properties of FRP are an ongoing concern. GFRP is a multiphase composite material with anisotropy. The mechanical properties of the resin matrix affect the efficiency of load transfer between fibers, which further affects the mechanical properties of GFRP. In addition, the smooth surface of glass fibers (GFs), which have few active functional groups, leads to suboptimal sizing effects between the GFs and the resin matrix [3]. These

performance shortcomings in the multiphase structure leads to weaker mechanical properties of GFRP. Currently, the mechanical properties of FRP are mainly enhanced by using high-performance fibers and improving resin-fiber interface properties. Glass fibers (GFs), while inferior in tensile properties to other reinforcing fibers such as carbon, basalt, and aramid, offer more economic benefits. The mechanical properties of FRP also depend on the performance of the resin matrix and the compatibility between the fibers and the resin matrix [4,5]. Sathishkumar et al. [6] summarized the influence of glass fiber types and content on the performance of GFRP. Various GFRP with good mechanical, tribological, thermal and vibrational properties have been used in electronics, aviation and automobile application etc. However,

\* Correspondence to: No. 777, Jialingjiang Eastern Road, Huangdao District, Qingdao City, China.

E-mail address: [baojiuwen@qut.edu.cn](mailto:baojiuwen@qut.edu.cn) (J. Bao).

<https://doi.org/10.1016/j.mtcomm.2024.110225>

Received 25 May 2024; Received in revised form 13 August 2024; Accepted 25 August 2024

Available online 26 August 2024

2352-4928/© 2024 Elsevier Ltd. All rights are reserved, including those for text and data mining, AI training, and similar technologies.

little attention has been paid to the effect of resin matrix on the mechanical properties of GFRP.

Various methods have been employed to enhance resin system performance, including nanomaterials, geopolymers, fibers, and functional curing agents [7]. Nanomaterials and functional curing agents have proven particularly effective in strengthening the resin system. Using carbon nanotubes, Pothnis et al. [8] increased the tensile strength of glass fiber-epoxy composites by 27 %. Xiao et al. [9] observed a synergistic effect of carbon nanotubes and nano-SiO<sub>2</sub> in enhancing the mechanical properties of epoxy resin. However, higher concentrations of nanomaterials tend to agglomerate, leading to increased porosity in the modified resin systems [10]. To address this issue, Yu et al. [11] prepared epoxy nanocomposites by grafting polyacrylic acid onto graphene, enhancing the dispersion of graphene in the resin and its compatibility with epoxy resin. This incorporation of polyacrylic acid-modified graphene resulted in a 41.04 % increase in tensile strength and a 43.23 % increase in elastic modulus. Fulmali et al. [12, 13] improved the stress transfer efficiency of resin matrix and sizing effect between resin and fibers by the use of carboxyl functionalized multiwalled carbon nanotubes, resulting in enhanced mechanical and durability-related properties of GFRP. Besides, Yang et al. [14] experimented with epoxy resin using three different curing agents. The resin cured with polypropylene glycol bis exhibited the lowest tensile strength (32.7 MPa) and elastic modulus (1.8 GPa) but a significantly higher elongation (62 %). In contrast, due to their crosslinked structures with more rigid segments, the other resin systems displayed higher tensile strength (72–77 MPa) and elastic modulus (2.9–3.2 GPa). To date, these modified resin systems haven't been used in the production of FRP. There has been limited research on how the chemical structure and mechanical characteristics of the resin matrix affect the mechanical properties of GFRP.

Typically, the interface compatibility between a resin matrix and fibers determines their adhesion properties, which are crucial for efficient load transfer across the matrix-fiber boundary. Various methods have been employed to augment interfacial bonding strength, including roughening, nanomaterials, plasma, and silane coupling treatments for fiber surface modification [15,16]. The type of surface treatment applied to GFs influences composites' interfacial bonding and failure strength [17]. Zhao et al. [18] enhanced the fiber-matrix interfacial adhesion significantly by grafting graphene oxide onto the surface of glass fiber fabric. Chen et al. [19] developed multifunctional MXene-coated GFs through a straightforward electrophoretic deposition process. This resulted in an 8.1 % increase in the tensile strength of the GFs and a 22.4 % increase in the interfacial shear strength of composites, attributed to the nanosheets bridging the fiber surface defects. De et al. [20, 21] modified fiber surface by nanofillers achieved through electrophoretic deposition technique, improving the interfacial bonding with epoxy matrix. CFRP exhibited higher delamination resistance, flexural strength and inter-laminar shear strength, even under a cryogenic condition. However, altering the fiber surface topography to achieve higher interfacial bonding strength remains challenging. In the case of glass fiber reinforcement, mechanical interlocking due to surface roughness is less significant [22]. Silane coupling treatment, on the other hand, effectively enhances interfacial strength through strong physical and chemical bonding between fibers and matrix. Murray et al. [23] modified GFs using a coupling-activator compound, promoting covalent bonding between fiber and resin matrix. This was due to chain growth from the activator moieties, leading to a 20–28 % increase in mechanical properties and a 10–30 % improvement in fracture toughness of composites. Due to the significant improvement in the interfacial interaction among constituents of nanocomposites, the mechanical properties of GFRP reinforced by silanized fibers and nanoclay were significantly improved [24]. Nonetheless, few studies have focused on improving the tensile properties of GFRP through multiphase structure modification.

Despite advances in understanding the mechanical properties of modified resin systems and GFs, the analysis of enhancement

mechanisms and the synergistic effect between each enhanced phase of GFRP still demands special attention. This study aims to improve the tensile properties of an epoxy resin matrix using modified nanomaterials (SiO<sub>2</sub>/TiO<sub>2</sub>) and functional curing agents. A silane coupling agent (SCA) is prepared for excellent compatibility and interfacial bonding between nanomaterials, the epoxy resin matrix, and GFs. This research investigates the modification mechanisms, microscopic morphology, and tensile properties of the enhanced epoxy resin systems, GFs, and GFRP laminates through a combination of macroscopic experimental data and microstructure analysis. FTIR determines compositional changes in the modified nanomaterials. The wettability of glass fiber surfaces is assessed using a Contact Angle Meter. Morphological and elemental changes in SCA-treated GFs are observed through SEM and EDX. Tensile properties of the resin, GF bundles, and GFRP laminates with different GF fabric layers (2, 4, 8 layers) are evaluated using a tensile method. Meanwhile, the modification mechanisms of the multiphase structure in GFRP are analyzed. This research holds practical and significant value in preparing high-performance GFRP composites.

## 2. Experimental program

### 2.1. Materials

The specification of raw materials utilized in this study are itemized in Table 1, encompassing epoxy resin (E51), three curing agents, silane coupler, nano-TiO<sub>2</sub>, nano-SiO<sub>2</sub>, and glass fiber fabrics. The resin system, comprising epoxy resin and low molecular weight polyamide 650 curing agent (PA650), exhibited lower tensile strength [25]; hence, modified nanomaterials were incorporated to enhance the system. The calculation method of the amount of curing agent in epoxy resin is as follows:

$$\text{Amount of curing agent} = \text{active hydrogen equivalent/epoxy equivalent} \times 100 \%$$

Based on prior test outcomes and the epoxy equivalent and active hydrogen equivalent weight in the resin system [26], four epoxy resin systems were selected in this study: (i) E51 and PA650 with a mass ratio of 1:1; (ii) E51, PA650, and modified SiO<sub>2</sub>/TiO<sub>2</sub> with a mass ratio of 50:50:1:1; (iii) E51 and phenolic amine curing agent (PAA) with a mass ratio of 2:1; (iv) E51 and alicyclic amine curing agent (AA) with a mass ratio of 2:1.

### 2.2. Silane coupling treatment of GFs and nanomaterials

Polar groups in the silane coupler (KH560) play a crucial role in bonding inorganic and organic materials, enhancing composites' interfacial properties. Silane coupling treatment for GFs and nanomaterials was executed using a solution dipping method. This approach prepared a 50 % ethanol-water solution (EtOH: H<sub>2</sub>O = 1:1). The silane coupler content in SCA was 2 % to avoid the self-polymerization of hydroxyl groups. The silane coupler was dissolved in the ethanol-water solution at a mass ratio of 1:49, and the solution's pH was adjusted to 4–5 by adding acetic acid. Stirring was continued for 30 minutes to fully hydrolyze the

**Table 1**  
The specification of materials used in this study.

Materials	Specification
E51	Diglycidyl ether bisphenol-A with an equivalent epoxy weight of 185–210 g/eq
PA650	The active hydrogen equivalent is 175–205 g/eq
PAA	The active hydrogen equivalent is 105–115 g/eq
AA	The active hydrogen equivalent is 100–110 g/eq
Nano-TiO <sub>2</sub> /Nano-SiO <sub>2</sub>	The particle size is 15 nm
Glass fiber fabrics	The areal density and thickness of glass fiber fabrics are 200 g/m <sup>2</sup> and 0.2 mm, respectively.
Silane coupler (KH560)	$\gamma$ -(2,3-epoxypropoxy) propyltrimethoxysilane

silane molecules into silanol groups at room temperature ( $22 \pm 2$  °C).

Before this treatment, the GFs underwent a cleaning process to remove surface impurities. Initially, pre-sized glass fiber fabrics were immersed in an acetone bath for 24 hours. Following repeated washing in distilled water with ultrasonication, the fabrics were dried in a vacuum oven at 50 °C for 24 hours. Subsequently, the cleaned glass fiber fabrics were immersed in the silane coupling agent (SCA) for one hour at room temperature ( $22 \pm 2$  °C) [27,28]. The modified glass fiber fabrics were finally acquired after drying in a vacuum oven at 50 °C for 24 hours.

To address the agglomeration issue of nanomaterials, nano-TiO<sub>2</sub> and nano-SiO<sub>2</sub> were modified using SCA. The production process of the modified nanomaterials and the epoxy resin matrix is depicted in Fig. 1. Considering the dispersion of nanomaterials in SCA, 20 wt% of nanomaterials were mixed into SCA and stirred continuously for five hours to ensure complete reaction with silanol groups. The modified nanomaterials were washed with anhydrous ethanol to avoid hydroxyl self-polymerization, and dried in a vacuum oven at 50 °C for 24 hours to avoid the adverse effects of moisture [29,30]. Due to agglomeration of nanomaterials after drying, the nanomaterials were mechanically treated at 300 rpm for 10 min using a planetary ball mill to obtain fine powders. The diameter of steel balls for grinding is 2, 3, 5 and 10 mm. Based on previous research, the resin system containing epoxy resin and PA650 was enhanced with 1 wt% modified nano-TiO<sub>2</sub> and nano-SiO<sub>2</sub>. Stirring was continued for 15 minutes to achieve a well-dispersed resin matrix.

### 2.3. Resin and GFRP laminate specimen preparation

Based on GB/T 2567 [31], four epoxy resin systems, named EPA650, EPA650-Md, EPAA, and EAA, were cured in silicone molds at room temperature ( $22 \pm 2$  °C) for one day. The standard length for resin tensile specimens was set at 50 mm. GFRP laminates were fabricated using the hand layup technique. During production, mild steel molds measuring  $350 \times 350 \times 50$  mm<sup>3</sup>, vacuum compression bags, and a vacuum pump were utilized. The self-manufactured laminates measured 300 mm × 300 mm in two-dimensional size, varying thickness based on the number of GF fabric layers and the resin matrix. This study prepared GFRP laminates with two, four, and eight-ply GF fabrics. The SCA-treated GF fabrics were used only with EPA650-Md. The other resin-based (EPA650, EPAA and EAA) GFRP laminates made with common GF fabrics. The resin matrix to glass fiber fabric mass ratio was maintained at 3:2. As per ASTM D3039 [32], the GFRP composites were

sectioned for various tests. The standard length for GFRP laminate tensile specimens was 100 mm. The resin and GFRP laminate specimens' detailed shapes and dimensions are depicted in Fig. 2. These laminate specimens were designated based on the resin system types and the number of GF fabric layers. For instance, EPA650-2 L denotes GFRP laminates with an EPA650 resin system and two GF fabric layers.

### 2.4. Test methods

The tensile properties of GFs, resin, and GFRP laminate specimens were evaluated using a universal testing machine at a displacement rate of 2 mm/min (see Fig. 3). Five samples were tested for each resin and GFRP laminate type to obtain average values under each condition. Additionally, fifty GF bundle samples, each with a 200 mm standard length, were prepared from untreated and treated glass fiber fabrics. The tensile behavior of GF bundles was analyzed using the Weibull distribution based on the weakest link theory [33]. As the interactions between nanomaterials, GFs, and SCA are not directly observable, FTIR, SEM, and EDX were employed to examine the surface changes of nanomaterials and GFs following SCA treatment. FTIR allowed for an indirect qualitative analysis of the reactions between nanomaterials and SCA based on changes in chemical bonds and functional groups. The chemical composition on the surface of GFs could be further identified both qualitatively and quantitatively using EDX. In addition, the apparent contact angle qualitatively assessed the sizing effect between the modified GFs and epoxy resin.

## 3. Results and discussions

### 3.1. Tensile behaviors of SCA-treated GF bundles

The tensile behaviors of both treated and untreated GF bundles were investigated through tensile tests. Fig. 4(a) reveals the correlation between GF bundles' ultimate tensile load and peak deformation. Due to the inherent brittleness of GFs, their tensile strength typically displays significant variability [34]. The ultimate tensile load for the modified GF bundles rose from 36–85 N to 50–94 N, which is attributed to the improvement of bonding between fibers. Fig. 4(b) shows that the GF bundles exhibited varied tensile behaviors post-SCA treatment. The enhanced GF bundles demonstrated higher ultimate tensile loads and rigidity due to the filling of SCA between fibers. In addition, the modified GFs were prone to brittle fractures under high loads. In contrast, individual fibers in untreated GF bundles, lacking this constraint, failed

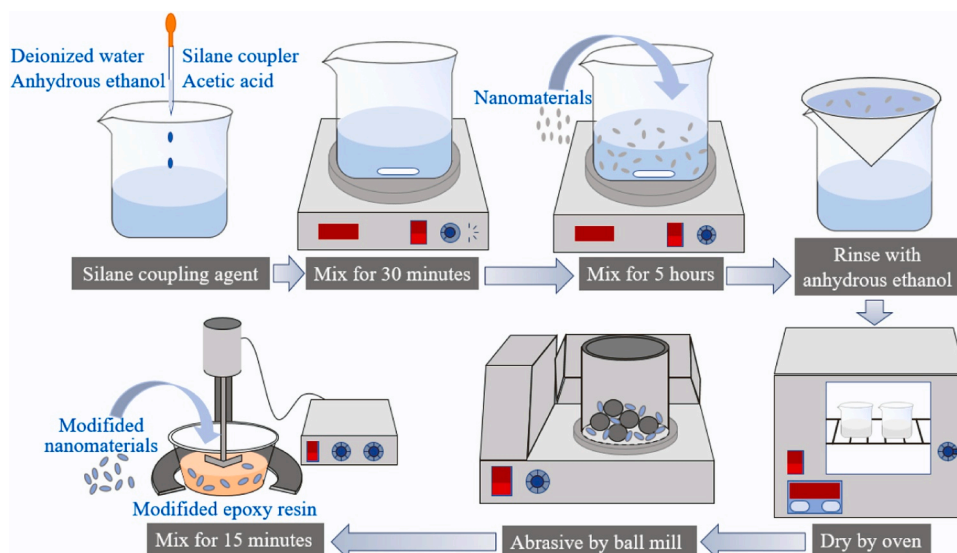


Fig. 1. The manufacturing process of modified nanomaterials and resin.

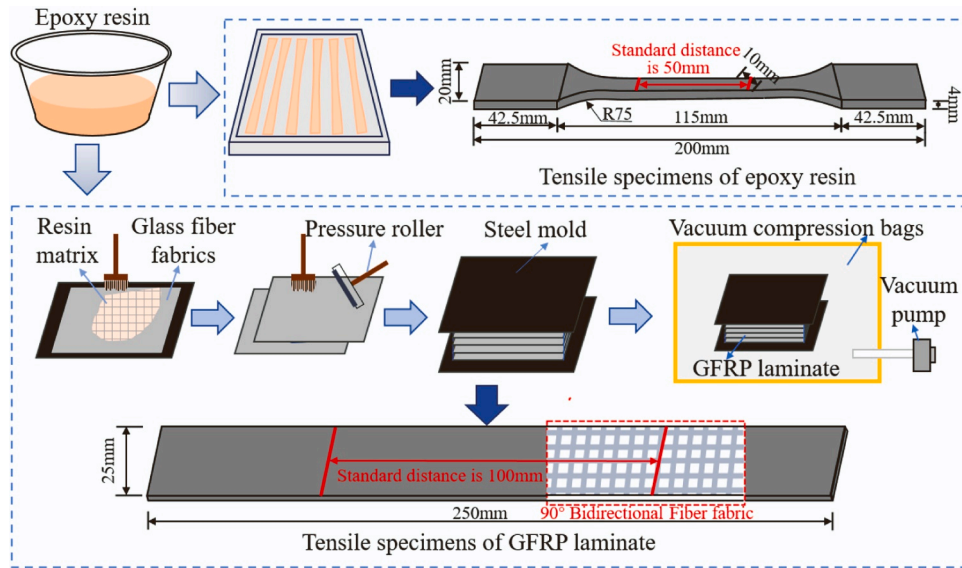


Fig. 2. The production process of epoxy resin and GFRP laminate specimens.

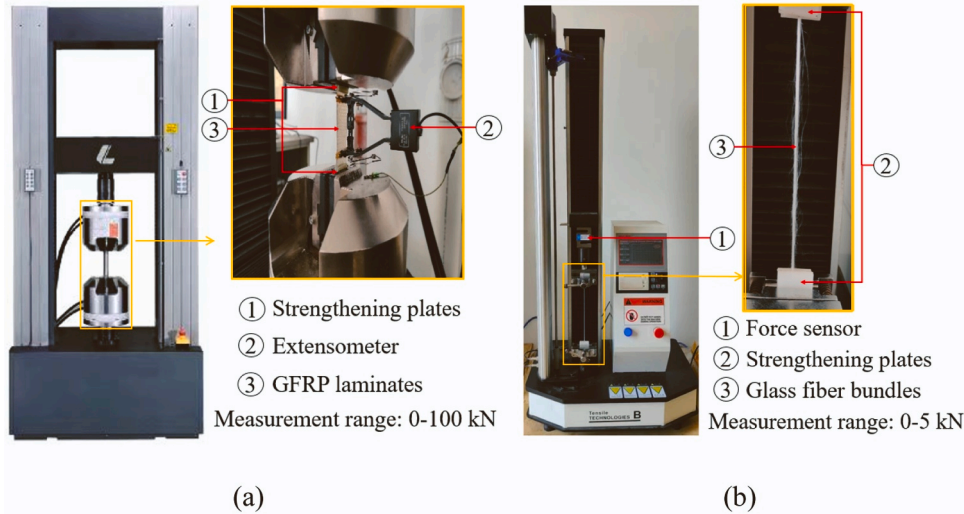


Fig. 3. Testing machines for (a) resin and GFRP, and (b) glass fiber bundles.

at varying deformations, leading to a progressive failure.

The brittle nature of GF bundles resulted in a stochastic distribution of their ultimate tensile load. A gage-length dependent Weibull distribution aptly characterizes the fiber tensile behaviors [35]. The fibers' cumulative failure probability is expressed as follows

$$F_{(\sigma,l)} = 1 - \exp\left[-\frac{l}{l_0}\left(\frac{\sigma}{\sigma_0}\right)^m\right] \quad (1)$$

where  $F_{(\sigma,l)}$  is the cumulative failure probability of a fiber of length  $l$  at a strength level of  $\sigma$ ;  $l_0$  is the reference gage length;  $\sigma_0$  and  $m$  are the experimentally determined Weibull scale and modulus parameters, respectively. Eq. (1) can be employed to scale the fiber strength to different gage lengths. In the case where all fiber specimens have the same length, the cumulative failure probability of fiber can be given by

$$F_{(\sigma)} = 1 - \exp\left[-\left(\frac{\sigma_i}{\sigma_0}\right)^m\right] = \frac{i}{N+1} \quad (2)$$

where  $i$  is the ranking of the specimen that broke at strength  $\sigma_i$ ;  $N$  is the total number of fiber specimens at that particular length. The ultimate

tensile load of GF bundles was ranked as  $i=1, 2, 3, \dots, N$  in increasing load order.

Fig. 5 depicts the Weibull parameter estimation for GF bundles. The fitting curves to the experimental data yielded the Weibull scale and modulus parameters. The scale parameter  $\sigma_0$  is the load at which 63.2 % of the fibers break ( $F_{(\sigma)} = 0.6321$ ). A higher value of  $m$  suggests that GF bundle failures occur within a more confined range of failure load [36]. The characteristic load  $\sigma_0$  experienced a 10.64 % increase in the treated GFs due to SCA's constraining effect. In addition, the rise in the Weibull modulus parameter  $m$  indicated that the ultimate tensile loads for GF bundles were concentrated in a narrower range. The SCA modification led to a modest improvement in the characteristic load of GF bundles and altered the fracture mode of the modified GF bundles.

### 3.2. Tensile properties of different epoxy resin systems

The tensile properties of four epoxy resin systems are illustrated in Fig. 6. According to GB/T 2567 [30], the ultimate tensile strength (UTS), elastic modulus, and breaking elongation are calculated. Previous studies [37] have shown that the UTS, breaking elongation, and elastic

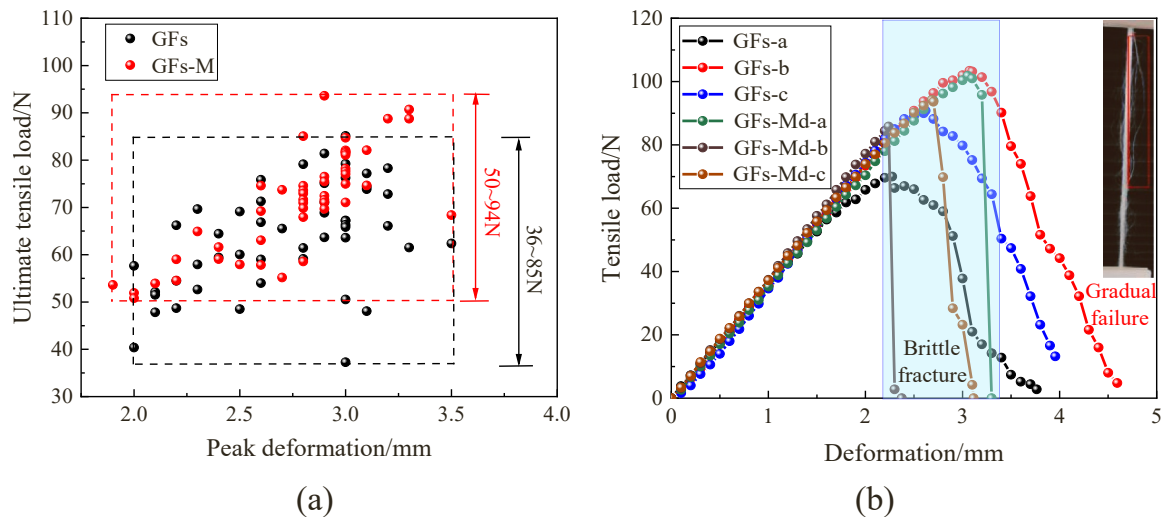


Fig. 4. Tensile behaviors of GF bundles: (a) the relationship between ultimate tensile load and peak deformation, and (b) tensile load-deformation curves.

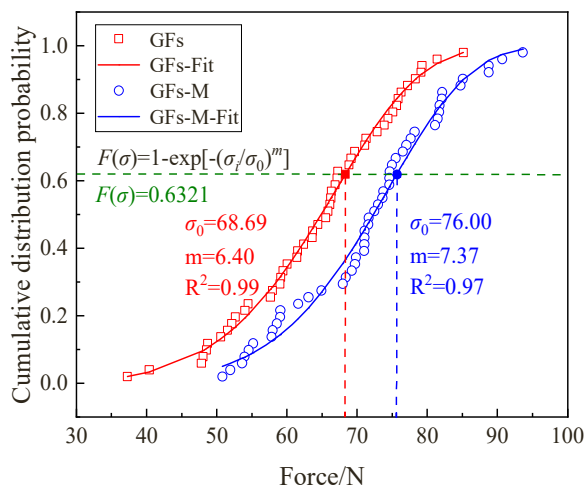


Fig. 5. Weibull parameter estimation of GF bundles.

modulus of TiO<sub>2</sub>/SiO<sub>2</sub>-modified epoxy resin decrease with an increase in nanoparticle weight percentage, primarily due to nanoparticle agglomeration. However, the breaking elongation of EPA650-Md

exhibited a significant increase of 55.41 %. This improvement is likely attributable to the functionalization of nanomaterials by SCA. The functional groups on the surface of these nanomaterials enhance dispersion and strengthen molecular interactions [38]. The resin systems, employing different curing agents, exhibit distinct chemical and crosslinking structures, which influence the tensile properties of the resin specimens. Notably, EPA650-Md demonstrated the highest breaking elongation (7.60–7.91 %) due to its flexible chain structure, while EPAA and EAA exhibited superior UTS (31.59–36.53 MPa and 37.82–41.43 MPa) and elastic modulus (3.61–3.72 MPa and 3.2–3.67 MPa). These resin systems (EPAA and EAA) possess a cross-linked structure with more rigid segments, enhancing tensile strength [39,40]. However, it is challenging for these resin systems to simultaneously achieve high strength and ductility. The UTS and elastic modulus of resins generally increase as breaking elongation decreases, mainly because of variations in the chemical structure of the resin systems.

The range of stress-strain curves and toughness values of the epoxy resin systems are depicted in Fig. 7. The tensile specimens with EPAA and EAA failed at higher stress, while those with EPA650-Md failed because of higher strain. The incorporation of nanomaterials notably affected the elastic modulus and ductility of EPA650. EPA650-Md showed an improved balance between strength and deformation compared to other resin systems. Numerical integration based on the

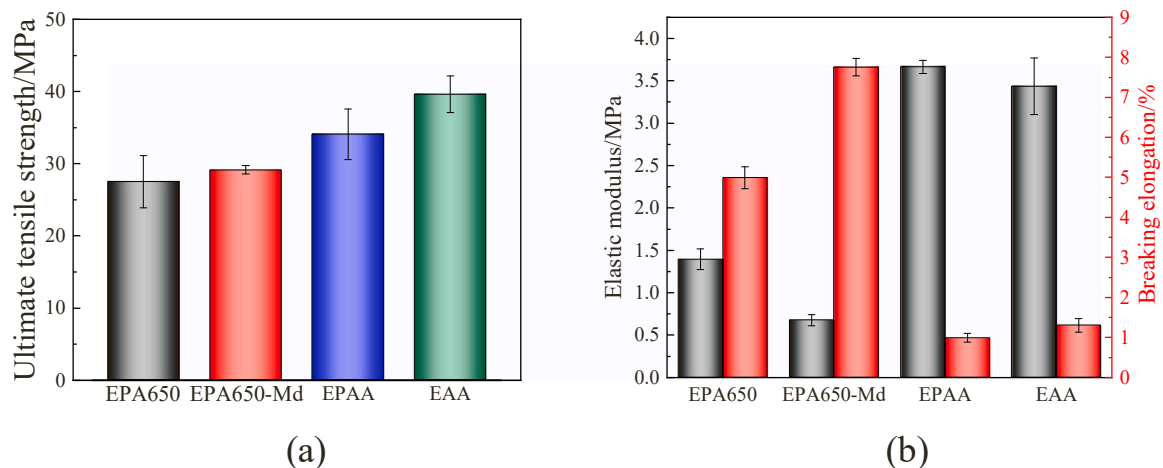


Fig. 6. Tensile properties of epoxy resin systems: (a) ultimate tensile strength and (b) elastic modulus and breaking elongation.

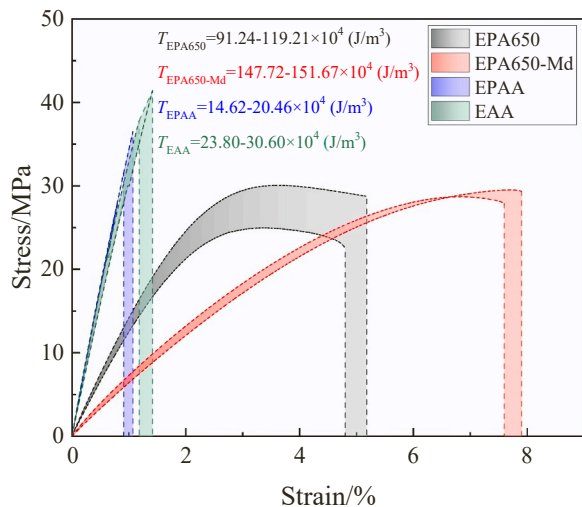


Fig. 7. Stress-strain curves and toughness of epoxy resin systems.

trapezoid method was used to calculate the toughness of epoxy resin systems as the area under the stress-strain curves shown in Fig. 7 [41]. In particular, the enhancement in toughness of EPA650-Md ( $147.72\text{--}151.67\text{ J/m}^3$ ) can be attributed to the effective bonding between the resin matrix and nanoparticles. The effect of functional nanomaterials on the enhancement of resins has been demonstrated in the previous studies [42,43]. Conversely, the toughness of EPAA and EAA markedly decreased due to their rigid structure.

### 3.3. Tensile properties of GFRP laminates based on different epoxy resin systems

#### 3.3.1. Influence of size effect in GFRP laminates

Modern fabrication technology enables the thinning of plies, offering several benefits, such as reduced void volume fractions and diminished interlaminar cracking. However, the thickness of the plies in laminates exerts notable influences on their mechanical properties [44].

The UTS of GFRP laminates with two, four and eight-ply GF fabrics is depicted in Fig. 8(a). The results indicate that GFRP laminates with four-ply GF fabrics achieved the highest UTS, except in specimens utilizing EPA650. Previous studies have shown that fiber breakages are the primary failure mechanisms in thinner laminates [45]. The breaking elongation of brittle glass fiber fluctuates within a certain range of 1–5%. Due to EPA650's high breaking elongation (4.80–5.18%), the GFs in EPA650-2 L could undergo more extensive deformation at lower stress. Consequently, as Fig. 8(b) and (c) demonstrates, EPA650-2 L exhibited the highest breaking elongation (1.96–2.04%). In laminates, GFs primarily bear the tensile load. Thus, EPA650-2 L exhibited the lowest UTS (66.17–68.46 MPa). As the GF fabric layers in laminates with EPA650 (EPA650-4 L and EPA650-8 L) increased, the UTS and elastic modulus improved. However, the breaking elongation of EPA650-4 L and EPA650-8 L decreased, which is attributable to EPA650's inferior tensile strength and poor resin-fiber interface properties. The highest UTS of GFRP with EPA650 was 121.37 MPa.

Due to the performance optimization of the multiphase structure (EPA650-Md and SCA-treated glass fiber fabrics) in GFRP, a significant improvement in the tensile properties of EPA650-Md-based GFRP laminates. The toughened resin matrix and improved fiber-resin interfacial adhesion contributed to this enhancement. EPA650-Md-2 L and EPA650-Md-4 L exhibited higher UTS (133.6–136.97 MPa and 157.12–169.79 MPa) and breaking elongation (2.05–2.25% and 1.99–2.11%) than EPA650-2 L and EPA650-4 L. However, the tensile properties of EPA650-Md-8 L decreased. As the ply thickness increases, the failure mechanisms of the laminates include fiber breakage and

fiber-matrix debonding [46], and the anisotropy of the multiphase structure leads to varying stress levels between layers. The highest stress was observed in the top and bottom layers, while the middle layers experienced reduced stress [47]. Despite the modification of EPA650 with nanomaterials, there is no increase in its tensile strength, making it difficult to transfer the tensile load effectively between fibers. Consequently, EPA650-8 L and EPA650-Md-8 L exhibited similar tensile properties. The overall performance of the EPA650-Md-4 L can be utilized due to the thinner thickness, which avoid uneven interlayer stresses. The improvement of resin toughness and fiber-resin interfacial performance can improve the tensile properties of GFRP. However, the UTS and elastic modulus of the resin matrix affects the efficiency of stress transfer between layers. It is necessary to investigate the effect of these factors on the tensile properties of GFRP.

The breaking elongation of EPAA-2 L (1.24–1.42%) and EAA-2 L (1.06–1.25%) is much smaller than EPA650-based GFRP (1.96–2.25%) because of EPAA's and EAA's rigid structures. But the UTS of both EPAA-2 L (125–147 MPa) and EAA-2 L (117.09–120.94 MPa) were improved compared to the EPA650-based GFRP. Due to the higher UTS and elastic modulus of EPAA and EAA, the load transfer efficiency between fibers was improved. GFRP laminates with four and eight glass fiber fabrics exhibited stable tensile properties. However, those resin systems cannot completely eliminate uneven loading between layers. The tensile properties of the laminates with eight-ply GF fabrics were slightly inferior to those with four-ply GF fabrics. The UTS and toughness of GFRP with four-ply GF fabrics were significantly improved by the use of EPAA and EAA.

The microstructural heterogeneity induced by bridging fibers and resin matrix may become the primary sources of the observed variations in mechanical fracture behaviors [48]. Fig. 9 indicates that GFRP laminates with two glass fiber fabrics failed due to the breakdown of the resin matrix. The GFs, unrestrained by the resin matrix, fractured readily. In laminates with four glass fiber fabrics, both GFs and the resin matrix failed, and the emergence of interfacial debonding between GFs and the resin matrix contributed significantly to laminate fractures. However, the lower UTS of EPA650 and EPA650-Md caused internal delamination in GFRP with eight-ply GF fabrics, resulting in ineffective load transfer between fibers. Although the tensile properties of GFRP can be improved by using EPAA and EAA, the uneven loading between layers cannot be completely eliminated. The uneven loading caused damage from outside to inside, reducing effective force area of GFRP. As a result, EPAA and EAA-based GFRP with eight-ply GF fabrics had a relatively flat tensile cross section at damage. Appropriate ply thickness of composites allows each phase in the GFRP to bear the tensile load simultaneously. Meanwhile, the uneven loading between layers in GFRP with eight-ply GF fabrics caused internal delamination and uneven destruction, reducing the tensile properties of laminates.

#### 3.3.2. Tensile properties of GFRP laminates with different resin systems

Due to the superior tensile properties of laminates composed of four-ply GF fabrics, researchers chose these specimens to examine the impact of different epoxy resin systems on tensile characteristics. Fig. 10 illustrates the tensile properties of GFRP laminates with varied epoxy resin systems. Fig. 10(a) and (b) indicate that the tensile properties of GFRP can be improved by the simultaneous use of toughened resins (EPA650-Md) and SCA-treated GF fabrics. As shown in Table 2, the UTS of GFRP with low strength resin systems (EPA and EPA-Md) increased with the resin breaking elongation of resin. However, the enhancement in tensile properties by EPA650-Md was partly limited due to its flexible chain structure. GFRP with EPAA and EAA exhibited the higher UTS, elastic modulus, and breaking elongation (1.9–2.1%) owing to rigid chemical structure.

Fig. 10(c) reveals that the ultimate strain of laminates can be enhanced by increasing the ductility (EPA650-Md), UTS and elastic modulus (EPAA and EAA) of the resin systems. Additionally, the improvement in fiber-resin interfacial adhesion further augments the

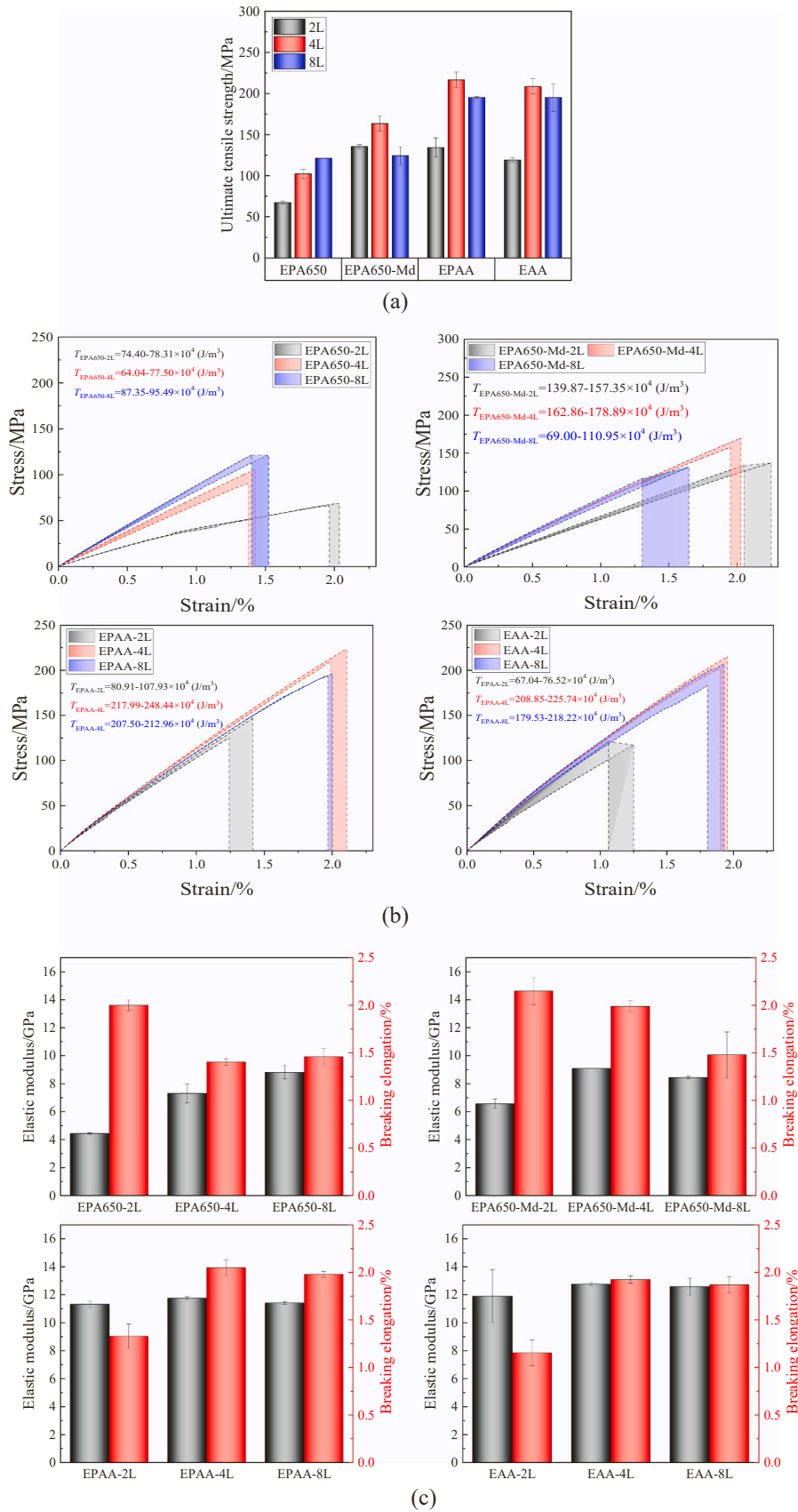


**Fig. 8.** Tensile properties of GFRP with different GF fabric layers: (a) Ultimate tensile strength, (b) stress-strain curves and toughness, and (c) elastic modulus and breaking elongation.

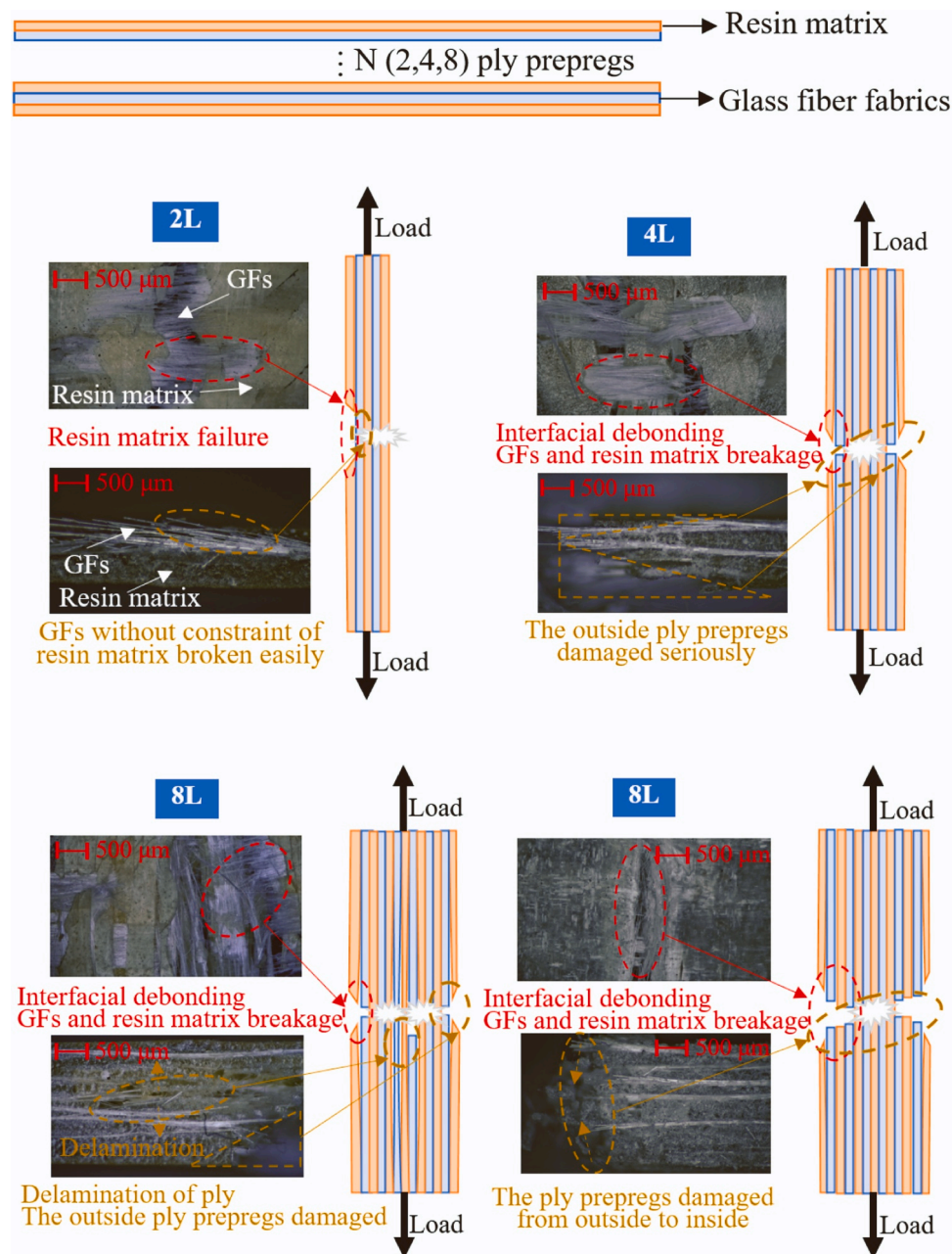


Fig. 9. Failure mechanisms of GFRP laminates with different GF fabric layers.

tensile properties of the laminates. EAA, possessing fewer reactive functional groups (-OH) than the EPAA resin system, resulted in weaker fiber-resin interfacial adhesion than EPAA-4 L. The increased number of reactive functional groups (-OH) in EPAA enhanced the bonding between GFs and the resin matrix, improving the tensile properties of EPAA-4 L. EPAA-4 L reflected a balance between strength and deformation, achieving the highest toughness value. As the UTS and elastic modulus of the resin matrix and the fiber-matrix interfacial adhesion increased, the tensile load was transferred more effectively across the matrix-fiber boundary. The expansion of debonding area in laminates with enhanced tensile properties indicated that each phase in the GFRP can fully bear the tensile load.

### 3.4. Enhancement mechanism analyses

#### 3.4.1. Determination of functional groups of SCA-treated nanomaterials

The composition of the epoxy resin is complex and the functional

groups in the SCA cannot be highlighted by FTIR. Thus, FTIR was employed to identify the functional groups added to the nanomaterials' surface by SCA. Fig. 11 displays a characteristic spectrum featuring the following major peaks: (a) a strong absorption band at  $468\text{ cm}^{-1}$  attributed to Si-O; an absorption band at  $810\text{ cm}^{-1}$  linked to Si-OH; an absorption band at  $1098\text{ cm}^{-1}$  from the Si-O-Si band [49]; (b) an absorption band in the  $500\text{--}700\text{ cm}^{-1}$  range due to Ti-O [50]. Absorption bands at  $950\text{ cm}^{-1}$  associated with  $\text{SiOCH}_3$ ,  $1010\text{--}1090\text{ cm}^{-1}$  due to  $\text{CH}_2\text{OCH}$ ,  $1022\text{ cm}^{-1}$  from the Si-O-Ti band, and two pronounced absorption bands at  $2860/2880$  and  $2930/2940\text{ cm}^{-1}$ , related to  $\text{CH}_2$  and  $\text{CH}_3$  vibrations of SCA, were detected in the SCA-treated nanomaterials, confirming the incorporation of SCA onto the nanomaterials' surface [51].

#### 3.4.2. Morphological properties

The surface structure and elemental composition of GFs were analyzed using SEM and EDX. SEM examination concentrated on

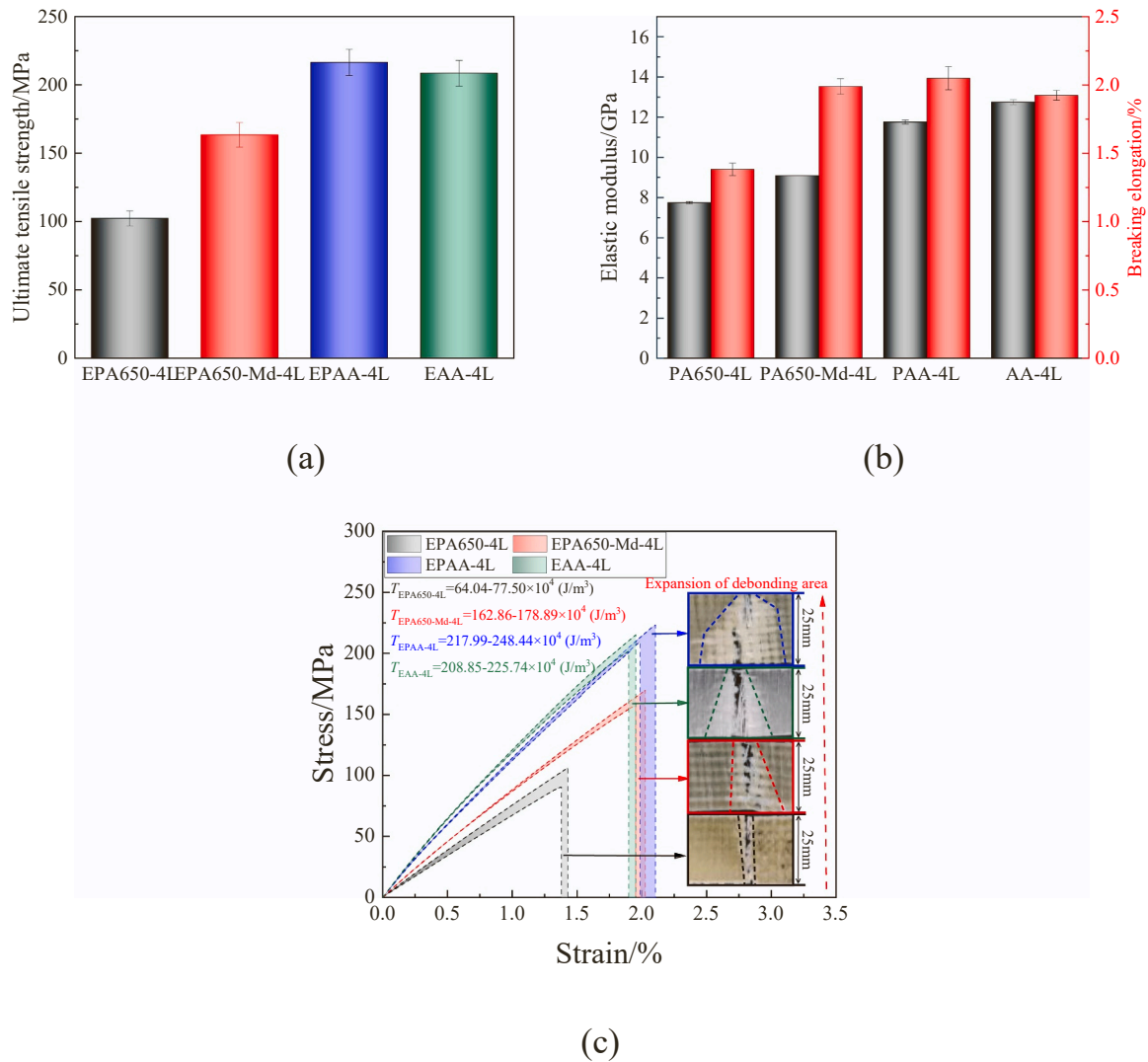


**Fig. 10.** Tensile properties of GFRP laminates with different epoxy resin systems: (a) ultimate tensile strength, (b) elastic modulus and breaking elongation, and (c) stress-strain curves and toughness.

**Table 2**

The UTS and breaking elongation of resin and laminates.

Sample name	UTS/MPa	Breaking elongation/%
GF	/	1–5
EPA650	25–30	4.8–5.2
EPA650-Md	28–30	7.6–7.9
EPA650–4 L	98–106	1.3–1.4
EPA650-Md–4 L	157–170	1.9–2.0
EPAA	32–37	0.9–1.1
EPAA–4 L	210–223	2.0–2.1
EAA	38–41	1.2–1.4
EAA–4 L	202–215	1.9–2.0

observing the topography of the GFs' surface, employing thermal emission electron optics. As illustrated in Fig. 12(a), the surface of untreated GFs appears smooth, resulting in weaker adhesion between the resin matrix and GFs. In contrast, the surface morphology of SCA-treated GFs, as shown in Fig. 12(b), is rougher than that of untreated GFs. This roughness enhances mechanical interlocking between the resin matrix and GFs. In addition, the SCA strengthened the bonding between fibers, resulting in the improvement of GF bundles' rigidity and tensile strength. EDX was employed to conduct a chemical elemental analysis of GFs, capitalizing on the fundamental spectroscopy principle that each

element possesses a unique atomic structure, manifesting as a distinct series of peaks in its electromagnetic emission spectrum. The silane-to-oxygen ratio in both untreated and treated GFs was quantified using EDX. An increased silane-to-oxygen ratio indicated the successful integration of SCA onto the GFs' surface. The roughness and chemical reaction bonding of the treated GFs had a synergistic effect, improving fiber-resin interfacial bonding strength.

#### 3.4.3. Contact angle between epoxy resin and GF bundles

The modified GFs' enhancement effect on the sizing of epoxy resin was assessed by measuring the contact angle between the epoxy resin and GF bundles. Fig. 13 indicates that the contact angle between the epoxy resin and GFs diminished as processing time increased. The contact angle between the epoxy resin and GF bundles was  $33.31^\circ$  before SCA treatment. After the SCA treatment for one hour, the contact angle between resin and GF bundles showed a significant reduction ( $24.42^\circ$ ). This decrease was attributed to incorporating polar groups, which allowed GFs to achieve a more effective sizing with epoxy resin.

#### 3.4.4. Enhancement mechanism of multiphase structure in GFRP

The silane coupler KH560 is comprised of a coupling-activator compound, with the formula  $Y-(R)n-Si-X$ . In this formula, X signifies a hydrolyzable coupling moiety ( $-OCH_3$ ) that can bond to the surfaces of

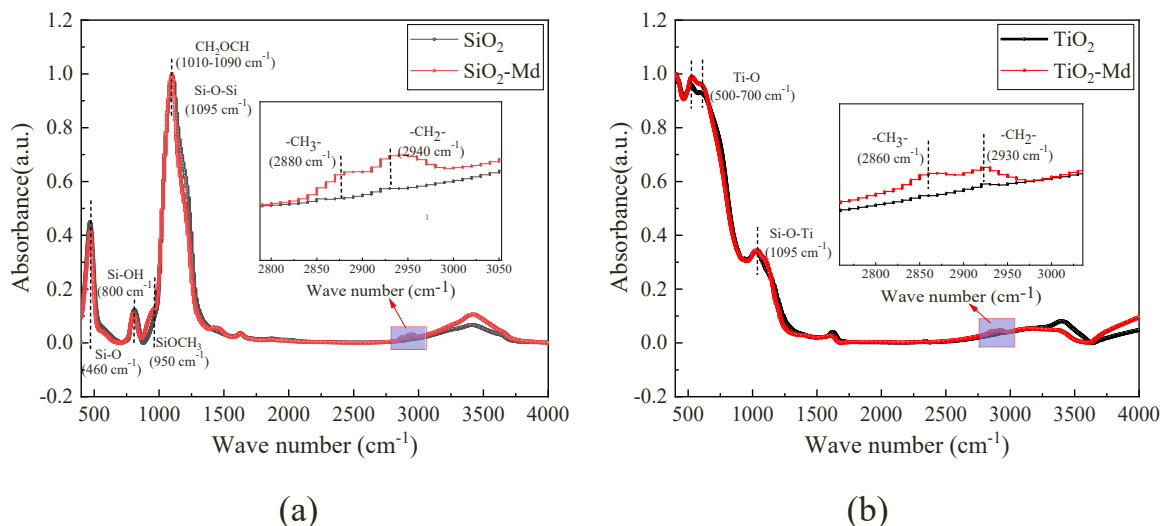


Fig. 11. FTIR spectra of silane coupling treated nanomaterials: (a) Nano-SiO<sub>2</sub> and (b) Nano-TiO<sub>2</sub>.

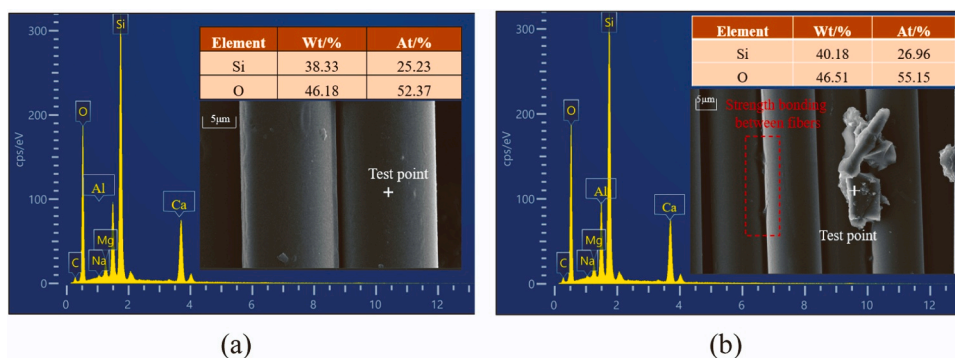


Fig. 12. SEM images and EDX analysis of (a) Untreated GFs and (b) SCA-treated GFs.

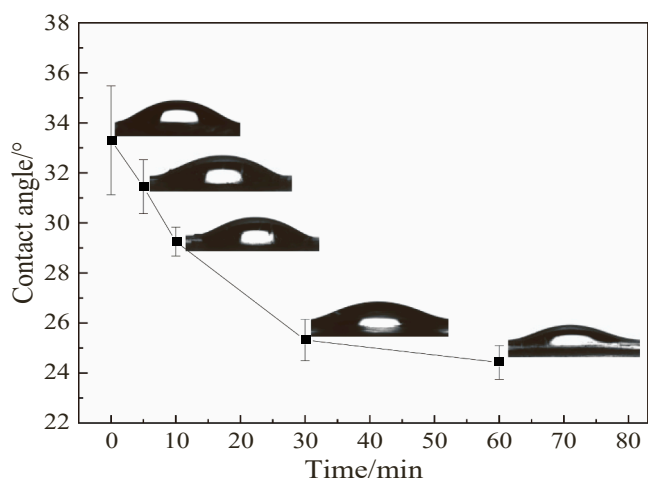


Fig. 13. Contact angle between epoxy resin and GFs bundles.

GFs and nanomaterials, Y denotes an epoxy group (-CH<sub>2</sub>(O)CH), and (R) n represents one or more polymerization activator moieties (-CH<sub>2</sub>-). Fig. 14(a) indicates that the X groups dissolved under specific conditions, resulting in the complete hydrolysis of silane molecules into silanol groups. SCA is synthesized via a dehydration condensation reaction of polar groups (-OH), as demonstrated in Fig. 14(b). In this process, the silanol groups in SCA can interact with the polar groups

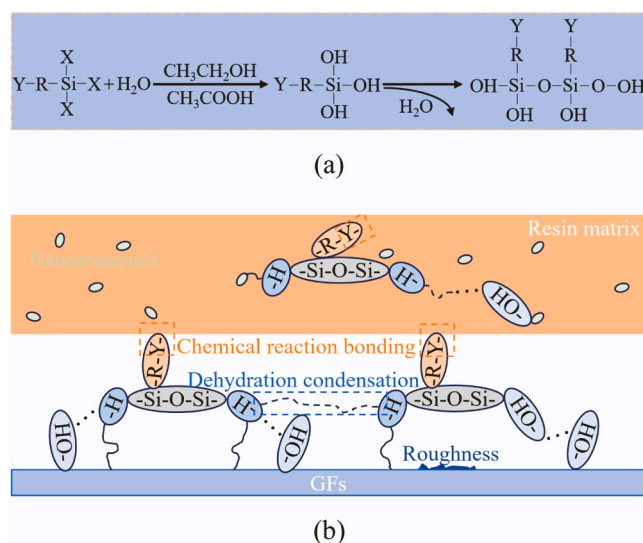


Fig. 14. Reaction mechanism of (a) SCA and (b) SCA-treated phase in GFRP.

(-OH) on the surfaces of GFs and nanomaterials. Subsequently, the Y groups in the SCA molecular chain can react with the epoxy resin matrix, enhancing the interfacial adhesion among nanomaterials, GFs, and the resin matrix. In addition, the increased roughness of the GFs' surface due to SCA treatment also enhances the mechanical interlocking force.

Collectively, these elements contribute to the improved tensile properties of the multiphase structure in GFRP.

#### 4. Conclusion

A comprehensive investigation combining macroscopic experimental data and microstructural analysis is conducted to evaluate the effect of multiphase structure optimization on the tensile properties of GFRP. The SCA can effectively modified the nanomaterials and GF, increasing the toughness of resin system, characteristic load of GF and wetting effect between GF and resin matrix. The resin system (EPA650) with long molecular chain achieved a greater ductility. Besides, the functional nanomaterials can further increase the breaking elongation of resin system (EPA650-Md). Conversely, the resin system with rigid elements and smaller molecular spacing between reactive functional groups (EPAA and EAA) showed a higher ultimate tensile strength and elastic modulus.

Laminates with four-ply GF fabrics facilitate more effective load transfer across the matrix-fiber interface, resulting in better tensile properties for GFRP. However, the uneven loading between layers in GFRP with eight-ply GF fabrics caused internal delamination and uneven destruction, reducing the tensile properties of laminates. In addition to the effect of ply thickness, the resin systems and interfacial performance had significantly influence in the tensile properties of GFRP. The tensile properties of GFRP improved by the simultaneous use of toughened resins (EPA650-Md) and SCA-treated GF fabrics, but the enhancement in tensile properties is partly limited due to flexible chain structure of the resin system. GFRP made of resin system (EPAA and EAA) with rigid elements exhibited the better tensile properties. Besides, more reactive functional groups (-OH) in EPAA enhanced the fiber-resin bonding, further improving the tensile properties of EPAA-4 L.

The main factors affected the tensile properties of GFRP were resin systems and interfacial performance between resin matrix and GF. The tensile properties of GFRP can be significantly improved by the use of functional nanomaterials, fibers and resin system. These factors increased the load transfer efficiency between resin-fiber boundary and ensured the performance of GF during the loading process. In the future researches, it is necessary to develop resin systems and functional fibers with more reactive groups and good mechanical properties. The utilization of these functional materials will significantly improve the performance and preparation efficiency of GFRP.

#### CRedit authorship contribution statement

**Yinlong Cao:** Writing – original draft, Data curation. **Guanghui Gao:** Validation, Data curation. **Peng Zhang:** Supervision, Funding acquisition. **Jiuwen Bao:** Writing – review & editing, Formal analysis, Conceptualization. **Peng Feng:** Methodology, Funding acquisition. **Rong Li:** Software, Methodology. **Wenhuan Wang:** Writing – review & editing, Formal analysis.

#### Declaration of Competing Interest

The authors declare that they have no known competing financial interests or personal relationships that could have appeared to influence the work reported in this paper.

#### Data Availability

The authors are unable or have chosen not to specify which data has been used.

#### Acknowledgements

The financial support for ongoing projects by the Natural Science Foundation of China (U2106219, 52378247, 51922052), Youth

Innovation Team Development Plan of Shandong Province in China (2021KJ019), Natural Science Foundation of Shandong Province (ZR2021JQ17) and Demonstration Project of Benefiting People with Science and Technology of Qingdao, China (Grant No. 24-1-8-cspz-9-nsh) are greatly acknowledged.

#### References

- [1] S. Zhang, T. Zhong, Q. Xu, Z. Su, M. Jiang, P. Liu, The effects of chemical grafting 1,6-hexanediol diglycidyl ether on the interfacial adhesion between continuous basalt fibers and epoxy resin as well as the tensile strength of composites, *Constr. Build. Mater.* 323 (2022) 126563.
- [2] K. Katagiri, S. Honda, S. Nakaya, T. Kimura, S. Yamaguchi, H. Sonomura, T. Ozaki, S. Kawakita, M. Takemura, K. Sasaki, Tensile strength of CFRP with curvilinearly arranged carbon fiber along the principal stress direction fabricated by the electrodeposition resin molding, *Compos. Pt. A-Appl. Sci. Manuf.* 143 (2021) 106271.
- [3] S. Keusch, R. Haessler, Influence of surface treatment of glass fibres on the dynamic mechanical properties of epoxy resin composites, *Compos Pt. A.* 30 (8) (1999) 997–1002.
- [4] M.S.H. Al-Furjan, L. Shan, X. Shen, M.S. Zarei, M.H. Hajmohammad, R. Kolahchi, A review on fabrication techniques and tensile properties of glass, carbon, and Kevlar fiber reinforced polymer composites, *J. Mater. Res. Technol.* 19 (2022) 2930–2959.
- [5] C. Li, Y. Dong, X. Yuan, Y. Zhang, X. Gao, B. Zhu, K. Qiao, Waterborne polyurethane sizing agent with excellent water resistance and thermal stability for improving the interfacial performance of carbon fibers/epoxy resin composites, *Colloids Surf. A-Physicochem. Eng. Asp.* 681 (2024) 132817.
- [6] T.P. Sathishkumar, S. Satheshkumar, J. Naveen, Glass fiber-reinforced polymer composites—a review, *J. Reinf. Plast. Comp.* 33 (13) (2014) 1258–1275.
- [7] X. Mi, N. Liang, H. Xu, J. Wu, Y. Jiang, B. Nie, D. Zhang, Toughness and its mechanisms in epoxy resins, *Prog. Mater. Sci.* 130 (2022) 100977.
- [8] J.R. Pothnis, D. Kalyanasundaram, S. Gururaja, Enhancement of open hole tensile strength via alignment of carbon nanotubes infused in glass fiber - epoxy - CNT multi-scale composites, *Compos. Pt. A-Appl. Sci. Manuf.* 140 (2021) 106155.
- [9] C. Xiao, Y. Tan, X. Yang, T. Xu, L. Wang, Z. Qi, Mechanical properties and strengthening mechanism of epoxy resin reinforced with nano-SiO<sub>2</sub> particles and multi-walled carbon nanotubes, *Chem. Phys. Lett.* 695 (2018) 34–43.
- [10] M. Al-Zu'bi, L. Anguilano, M. Fan, Effect of incorporating carbon- and silicon-based nanomaterials on the physico-chemical properties of a structural epoxy adhesive, *Polym. Test.* 128 (2023) 108221.
- [11] J. Yu, J. Chen, K. He, L. Liang, Z. Tian, Enhancement mechanism of epoxy resin by polyacrylic acid-modified 3D porous graphene: A microscopic and molecular dynamics perspective, *Compos. Sci. Technol.* 245 (2024) 110363.
- [12] A.O. Fulmali, R.N. Kar, B.C. Ray, R.K. Prusty, Superior flexural, interlaminar-shear and fracture performance of glass fiber/epoxy laminates employing 3-D reinforcement approach: Emphasis on through thickness functionalized CNT alignment, *Compos. Pt. A-Appl. Sci. Manuf.* 175 (2023) 107795.
- [13] A.O. Fulmali, S. Patnaik, D.K. Rathore, D. Bhattacharjee, B. Gwalani, B.C. Ray, R. K. Prusty, Enhanced extreme temperature bending and delamination resistance of GFRP composites through z-directional aligned nano-reinforcement: Emphasizing the effects of CNT functionalization, *Compos. Sci. Technol.* 244 (2023) 110272.
- [14] K. Yang, Z. Wu, C. Zhou, S. Cai, Z. Wu, W. Tian, S. Wu, R.O. Ritchie, J. Guan, Comparison of toughening mechanisms in natural silk-reinforced composites with three epoxy resin matrices, *Compos. Pt. A-Appl. Sci. Manuf.* 154 (2022) 106760.
- [15] Q. Wang, S. Chen, S. Zeng, P. Chen, Y. Xu, W. Nie, Y. Zhou, Tunable mechanical properties of glass fiber/epoxy composites by incorporating bioinspired montmorillonite-carbon nanotube/epoxy interface layer around the fiber, *Compos. Pt. B-Eng.* 242 (2022) 110092.
- [16] H. Cui, M.R. Kessler, Pultruded glass fiber/bio-based polymer: Interface tailoring with silane coupling agent, *Compos. Pt. A-Appl. Sci. Manuf.* 65 (2014) 83–90.
- [17] E.N. Brown, A.K. Davis, K.D. Jonnalagadda, N.R. Sottos, Effect of surface treatment on the hydrolytic stability of E-glass fiber bundle tensile strength, *Compos. Sci. Technol.* 65 (1) (2005) 129–136.
- [18] J. Zhao, S. Zhang, X. Ke, A. Pan, Q. Zhou, S. Zeng, P. Chen, Y. Xu, W. Nie, Y. Zhou, Simultaneously tuning interfacial and interlaminar properties of glass fiber fabric/epoxy laminated composites via modifying fibers with graphene oxide, *Compos. Sci. Technol.* 235 (2023) 109970.
- [19] X. Chen, Y. Hui, J. Zhang, Y. Wang, J. Zhang, X. Wang, S. Cheng, K. Wen, Z. Li, C. Yi, J. Shao, Single multifunctional MXene-coated glass fiber for interfacial strengthening, damage self-monitoring, and self-recovery in fiber-reinforced composites, *Compos. Pt. B-Eng.* 259 (2023) 110713.
- [20] S. De, A.O. Fulmali, K.C. Nuli, R.K. Prusty, B.G. Prusty, B.C. Ray, Improving delamination resistance of carbon fiber reinforced polymeric composite by interface engineering using carbonaceous nanofillers through electrophoretic deposition: An assessment at different in-service temperatures, *J. Appl. Polym. Sci.* 138 (2021) e50208.
- [21] S. De, P.N. Shivangi, S. Choudhury, A.O. Fulmali, B.C. Ray, R.K. Prusty, Effects of fiber surface grafting by functionalized carbon nanotubes on the interfacial durability during cryogenic testing and conditioning of CFRP composites, *J. Appl. Polym. Sci.* 138 (42) (2021) e51231.
- [22] P. Kiss, W. Stadlbauer, C. Burgstaller, V. Archodoulaki, Development of high-performance glass fibre-polypropylene composite laminates: Effect of fibre sizing

- type and coupling agent concentration on mechanical properties, *Compos. Pt. A- Appl. Sci. Manuf.* 138 (2020) 106056.
- [23] J.J. Murray, A. Bajpai, J. Quinn, J. McClements, K. Gleich, E.D. McCarthy, C. M. Brádaigh, Effect of glass fibre sizing on the interfacial properties of composites produced using in-situ polymerised Polyamide-6 transfer moulding, *Compos. Pt. B-Eng.* 235 (2022) 109743.
- [24] D. Shelly, T. Nanda, R. Mehta, Novel epoxy-based glass fiber reinforced composites containing compatibilized para-aramid fibers and silanized nanoclay for improved impact strength, *Polym. Compos.* 43 (3) (2022) 1357.
- [25] P. Deepak, R.V. Kumar, S. Badrinarayanan, H. Sivaraman, R. Vimal, Effects of Polyamide and/or Phenalkamine Curing Agents on the Jute Fibre Reinforcement with Epoxy Resin Matrix (Part A), *Mater. Today-Proc.* 4 (2) (2017) 2841–2850.
- [26] Z. Fadlurrahman, D. Alandro, G.N.C. Santos, M.A. Muflikhun, Mechanical and chemical properties of matrix composite: curing agent ratio, degassing process, and filler effect perspectives, *J. Eng. Res.* 11 (4) (2023) 488–497.
- [27] Y. Yang, H. Zhang, X. Liu, Y. Deng, M. Sun, J. Wang, Y. Cui, L. Pan, Z. Chen, Hierarchical interface design of jute fibers/polypropylene composites for enhanced interfacial and mechanical properties, *J. Clean. Pro.* 450 (2024) 141966.
- [28] Z. Chen, Q. Tu, X. Shen, Z. Fang, S. Bi, Q. Yin, X. Zhang, Enhancing the thermal and mechanical properties of carbon fiber/natural rubber composites by co-modification of dopamine and silane coupling agents, *Polym. Test.* 126 (2023) 108164.
- [29] Z. Li, H. Yan, F. Zhang, Hydrophobicity of montmorillonite synergistically controlled by silanization and aliphatic amine modification, *Colloid Surf., A: Physicochem. Eng. Asp.* 694 (2024) 134185.
- [30] J. Yang, H. Cui, Y. Zhang, R. Xu, X. Chen, J. Zhao, L. Dai, J. Guo, Y. Sun, A. Wang, L. Li, G. Sun, A double-layer multifunctional superhydrophobic coating with excellent anti-corrosion performance based on fluorine-free chemicals, *Prog. Org. Coat.* 187 (2024) 108150.
- [31] GB/T 2567, Test methods for properties of resin casting body, Natl. Stand Peoples Repub, China, 2021.
- [32] American Society for Testing and Materials (ASTM), Standard Test Method for Tensile Properties of Polymer Matrix Composite Materials (ASTM D3039), ASTM, West Conshohocken, PA, 2017.
- [33] Y. Paramonov, J. Andersons, A family of weakest link models for fiber strength distribution, *Compos. Pt. A- Appl. Sci. Manuf.* 38 (4) (2007) 1227–1233.
- [34] R. Ganesh, A.A. Obaid, J.W. Gillespie, Experimental determination of bimodal strength distribution of S-glass fibers, *Compos. Pt. B-Eng.* 254 (2023) 110559.
- [35] J.L. Thomason, On the application of Weibull analysis to experimentally determined single fibre strength distributions, *Compos. Sci. Technol.* 77 (2013) 74–80.
- [36] C. Scheffler, T. Förster, E. Mäder, G. Heinrich, S. Hempel, V. Mechtcherine, Aging of alkali-resistant glass and basalt fibers in alkaline solutions: Evaluation of the failure stress by Weibull distribution function, *J. Non-Cryst. Solids* 355 (52–54) (2009) 2588–2595.
- [37] A. Takari, A.R. Ghasemi, M. Hamadani, M. Sarafrazi, A. Najafidoust, Molecular dynamics simulation and thermo-mechanical characterization for optimization of three-phase epoxy/TiO<sub>2</sub>/SiO<sub>2</sub> nano-composites, *Polym. Test.* 93 (2021) 106890.
- [38] S.K. Singh, A. Kumar, S. Singh, A. Kumar, A. Jain, Investigation of thermo-mechanical properties of surface treated SiO<sub>2</sub>/epoxy nanocomposite, *Mater. Today-Proc.* 38 (Part 5) (2021) 2861–2865.
- [39] T. Maity, B.C. Samanta, S. Dalai, A.K. Banthia, Curing study of epoxy resin by new aromatic amine functional curing agents along with mechanical and thermal evaluation, *Mater. Sci. Eng. A.* 464 (1–2) (2007) 38–46.
- [40] R. Shree, R.B. Naik, R. Naik, G. Gunasekaran, R. Nimje, D. Ratna, Dual curing agents for optimized flame-retardancy and physico-mechanical properties of cycloaliphatic epoxy coating, *Mater. Chem. Phys.* 295 (2023) 127136.
- [41] B.S. Mustafa, G.M. Jamal, O.G. Abdullah, Improving the tensile, toughness, and flexural properties of epoxy resin based nanocomposites filled with ZrO<sub>2</sub> and Y<sub>2</sub>O<sub>3</sub> nanoparticles, *Results Phys.* 38 (2022) 105662.
- [42] J. Zhao, X. Xue, J. Wang, Y. Zhang, Y. Mi, Y. Zhang, Preparation and size control of epoxy resin multilevel structures with SiO<sub>2</sub> particles, *Colloids Surf., A: Physicochem. Eng. Asp.* 701 (2024) 134837.
- [43] S. Li, D. Chen, C. Gao, Y. Yuan, H. Wang, X. Liu, B. Hu, J. Ma, M. Liu, Z. Wu, Epoxy-functionalized polysiloxane/Nano-SiO<sub>2</sub> synergistic reinforcement in cryogenic mechanical properties of epoxy and carbon fiber reinforced epoxy laminate, *Compos. Sci. Technol.* 198 (2020) 108292.
- [44] Y. Zhou, C. Wang, J. Zhang, H. Wu, Experimental and theoretical investigation on tensile properties and fracture behavior of carbon fiber composite laminates with varied ply thickness, *Compos. Struct.* 249 (2020) 112543.
- [45] X. Li, Y. Yuan, Hybrid and gradient design of ultra-thin-ply composite laminates for synergistic suppression of delamination and fiber fracture damage modes, *Eng. Fract. Mech.* 295 (2024) 109822.
- [46] K. Al-Adily, M. Albdiry, H. Ammash, Evaluation of tensile and flexural properties of woven glass fiber/epoxy laminated composites oriented in edgewise and flatwise directions, *Ain Shams Eng. J.* 14 (12) (2023) 102255.
- [47] S.M. Shohel, S.H. Riyad, A.A. Noman, Study to analyze the mechanical strength of composite glass fiber laminated with resin epoxy, resin polyester, and PVC foam under tensile loading conditions by numerically using finite element analysis via Ansys, *Mater. Today-Proc.* (2023).
- [48] G. Frossard, J. Cugnoni, T. Gmür, J. Botsis, Ply thickness dependence of the intralaminar fracture in thin-ply carbon-epoxy laminates, *Compos. Pt. A- Appl. Sci. Manuf.* 109 (2018) 95–104.
- [49] A. Dhaffouli, P.A. Salazar-Carballo, S. Carinelli, M. Holzinger, H. Barhoumi, Improved electrochemical sensor using functionalized silica nanoparticles (SiO<sub>2</sub>-APTES) for high selectivity detection of lead ions, *Mater. Chem. Phys.* 318 (2024) 129253.
- [50] O. Sadek, S. Touhtouh, M. Rkhis, A. Hajjaji, Study of the hydroxylation of the TiO<sub>2</sub> thin layer prepared by spin-coating method using FTIR analysis and DFT theory, *Inorg. Chem. Commun.* 161 (2024) 112092.
- [51] J. Li, S. Li, Thermal and dielectric properties of epoxy resin filled with double-layer surface-modified boron nitride nanosheets, *Mater. Chem. Phys.* 274 (2021) 125151.